Detection of microvascular damage of membranous nephropathy by MicroFlow imaging: a novel ultrasound technique

Renjie Lu#, Fangfang Sun#, Lili Zhang, Chao Zhang, Jie Du, Jianxun Hao, Lirong Zhao

Department of Diagnostic Ultrasound Center, the First Hospital of Jilin University, Changchun, China

Contributions: (I) Conception and design: R Lu, L Zhao; (II) Administrative support: F Sun, L Zhang; (III) Provision of study materials or patients: R Lu, C Zhang; (IV) Collection and assembly of data: F Sun, L Zhao; (V) Data analysis and interpretation: J Du, J Hao; (VI) Manuscript writing: All authors; (VII) Final approval of manuscript: All authors.

#These authors contributed equally to this work as co-first authors.

Correspondence to: Professor Lirong Zhao, MD, PhD. Department of Diagnostic Ultrasound Center, the First Hospital of Jilin University, Changchun 130021, China. Email: zhaolir@jlu.edu.cn.

Background: MicroFlow imaging (MFI) is a novel noninvasive ultrasound (US) technique that depicts microcirculatory blood vessels in the kidney while filtering out tissue motion and enhancing blood flow signals. We aimed to investigate the value of MFI for the detection of renal microvascular perfusion in chronic kidney disease caused by stage I–II membranous nephropathy (MN).

Methods: Seventy-six participants including biopsy-proven MN (n=38) and healthy volunteers (n=38) were prospectively examined using MFI from March 2020 to December 2020. In addition, patients with MN were subdivided into a mild group, a moderate group, and a severe group based on the results of vascular pathology evaluation. All MFI images were analyzed by Image Pro Plus to obtain a cortical vascular index (VI). Basic patient information, relative US parameters and laboratory results were then acquired for each participant. Finally, after the univariate analysis among multiple groups, binary logistic regression (forward LR) and ordered logistic regression were used for multivariate analysis. Significance was set at P<0.05.

Results: VI was significantly lower in MN patients compared with that of healthy controls (0.65±0.09 *vs.* 0.35±0.18, P<0.001). After multivariate analysis, we found that the exploratory diagnostic performance of VI [area under the curve (AUC): 0.94; 95% confidence interval (CI): 0.89–0.99] outperformed that of serum creatinine (Scr) (AUC: 0.87; 95% CI: 0.79–0.95) in identifying MN. We also observed considerable differences among MN groups in parameters including VI (P=0.006), estimated glomerular filtration rate (eGFR) (P=0.037), shape (P=0.013), and impression (P=0.007). In addition, in the group with mild vascular damage, the exploratory diagnostic performance of VI (AUC: 0.79; 95% CI: 0.64–0.94) was better than other parameters, such as eGFR (AUC: 0.63; 95% CI: 0.43–0.84).

Conclusions: MFI detected abnormal renal microvascular perfusion in patients with MN (particularly in those with early vascular damage or preserved renal function) without the use of a contrast agent. Combining MFI with B-mode US can improve the predictive performance of traditional kidney US.

Keywords: MicroFlow imaging technology (MFI technology); ultrasound (US); membranous nephropathy (MN); chronic kidney disease

Introduction

Membranous nephropathy (MN) is a common cause of nephrotic syndrome, which comprises a group of diseases characterized histomorphologically by the thickening of glomerular capillary walls (1,2). Due to the damage to the walls of glomerular capillaries and arterioles, the renal function of MN patients can progressively deteriorate as the renal blood flow is altered (3). In approximately one third of patients with MN, the estimated glomerular filtration rate (eGFR) decreases with the progression of chronic kidney disease (CKD), ultimately progressing to end-stage renal failure (ESRD) (3,4). The number of patients with MN in China has increased from 10.4% to 24.1% between 2003–2006 and 2011–2014, respectively, and increased by more than two times in the 14–24 age category (5).

The onset of MN is occult, and initial clinical signs of this disease are subtle. Affected patients may present with discomfort, hypertension, edema of the eyes or lower limbs, proteinuria, or hematuria (1,3,4). The histopathologic changes are irreversible in most patients; however, if patients obtain a prompt diagnosis with early initiation of treatment, only 10% or less of these patients will develop ESRD (4). Because of increased compensatory kidney workload in kidney injury, early diagnosis is not heavily reliable on clinical, laboratory or gray-scale ultrasound (US) findings. PLA2R, a protein on human podocyte membranes, is a specific target antigen for idiopathic MN (IMN), discovered by Beck *et al.* in 2009 (6), and 70–80% of patients with IMN have circulating antibodies against PLA2R (1,7). However, because of the false-negative rate of PLA2R a negative serum PLA2R alone is not enough to exclude a diagnosis of PLA2R-associated MN (8,9). At present, only renal biopsy is used as a reference standard for a definitive diagnosis and stages of MN (10). However, this invasive procedure has the risk of serious complications (11-13). The renal biopsy may not be the preferred method for preliminary diagnosis, especially some patients at early proteinuria with microalbuminuria owing to the fact that renal biopsy has low acceptance among patients and cannot be used for periodic repeat examinations. Hence, novel noninvasive and quantitative imaging approaches that are sensitive to changes in renal structure are urgently needed for the preliminary detection of MN.

MicroFlow imaging (MFI) technology is an innovative method for visualizing the microcirculation of an anatomical formation without contrast media. Currently, MFI has been used to evaluate the microcirculation of superficial space-occupying lesions, muscle, joint ligament related diseases, improving the ability of US diagnosis and assessment, such as breast, carpal tunnel syndrome, and so on (14,15). It can also be applied to arterial plaque stability prediction, liver disease blood perfusion evaluation, chronic kidney allograft damage, and other aspects (16-19). MFI is a technique that can suppress the low-speed clutter caused by tissue movement and can be used to detect the lower-speed and finer blood-flow signals than those detected by color, power, and spectral Doppler, which lowers the necessity of subsequent contrast-enhanced US (CEUS) (20-22). A recent study has shown that MFI is a noninvasive method that can be used to quantify tissue vascular index [VI defined as the ratio of Doppler signal pixels to total pixels in the region of interest (ROI)] and shape for evaluating cortical perfusion damage (23). Microvascular damage is the crucial pathological change for the MN patients. MFI not only can visualize but also quantify renal blood flow and perfusion even in the small renal arterioles and capillaries. In our present study, we hypothesized that MFI can be used to identify differences in renal cortical perfusion between patients with MN and healthy controls. Hence, our aim in this study was to assess the predictive performance of MFI in the detection of MN and investigate the utilization of MFI in evaluating the extent of microcirculatory damage. We present this article in accordance with the STARD reporting checklist (available at https://qims.amegroups.com/article/view/10.21037/qims-23-1010/rc).

Methods

This prospective study was conducted between March 2020 and December 2020. The protocol used in this study was approved by the Ethical Committee of the First Hospital of Jilin University. The study was conducted in accordance with the Declaration of Helsinki (as revised in 2013). Written informed consent for a native kidney biopsy and participation in the study in its entirety was obtained from all the study participants. During this study, two radiologists used B-mode US, color Doppler, spectral Doppler, and MFI to evaluate 65 patients who had undergone a US-guided core needle kidney biopsy. Exclusion criteria included inability to acquire a high-quality US image, incomplete clinical or laboratory information, contraindications of renal puncture, other causes of chronic kidney disease and other stage MN besides stage I–II MN (*Figure 1*). Then, we recruited 38 healthy volunteers of similar age who had a physical examination at our hospital. Finally, 38 patients and
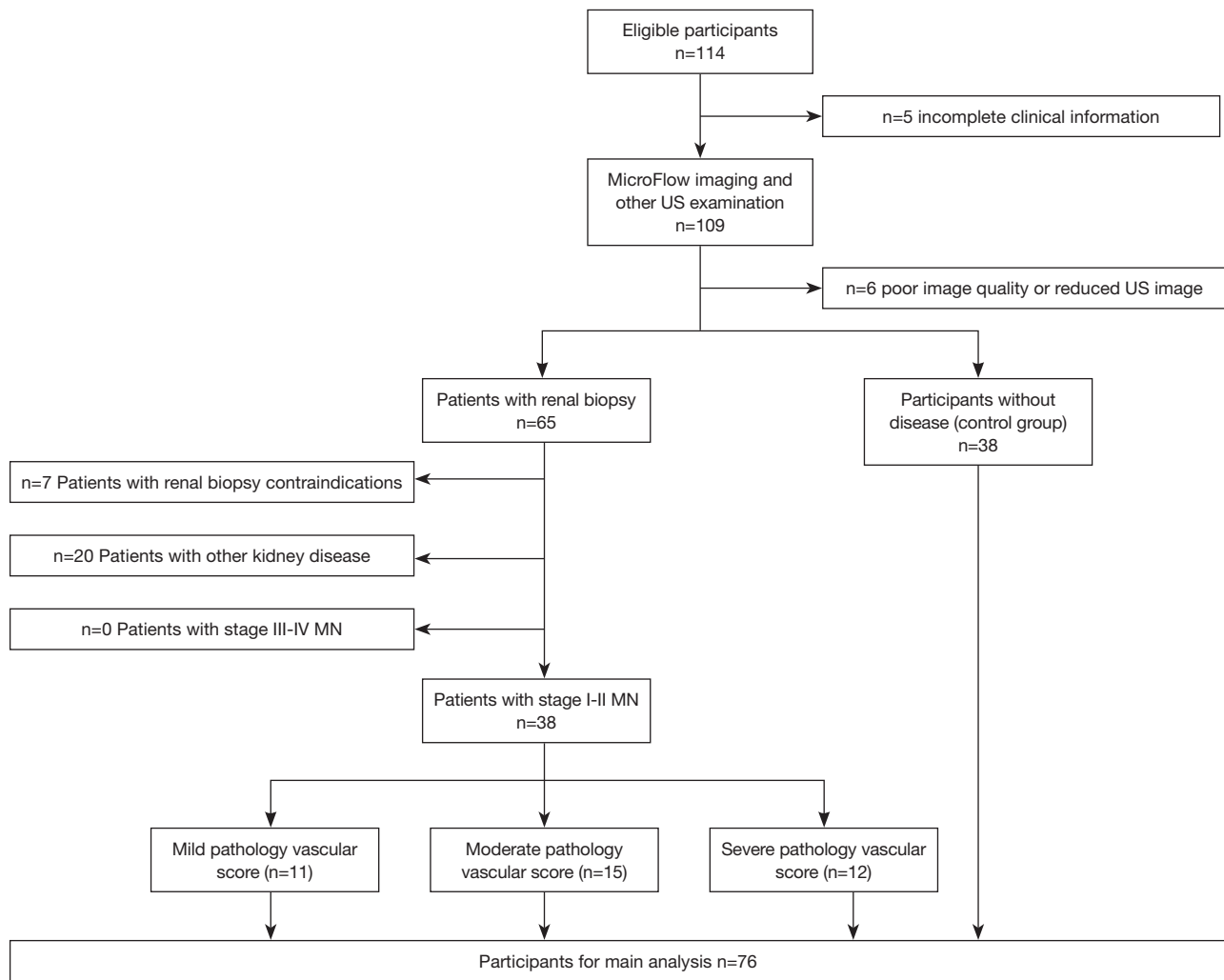
Figure 1 Study flowchart. US, ultrasound; MN, membranous nephropathy.

38 healthy volunteers were enrolled in our present study. The basic characteristics and laboratory results of all study participants are summarized in *Table 1*.

US examinations

All US examinations were performed using the same US equipment (Philips EPIQ5 color Doppler US diagnostic apparatus, Philips Healthcare, Andover, MA, USA; and C5-1 convex transducer, at a frequency of 4–6 MHz). The suite of tools, used for the evaluation of vessels and hemodynamics, included the following: color Doppler imaging, pulsed wave Doppler and MFI. Integral US evaluation of the kidney was performed during the preoperative period (morning of the biopsy or on the day before the biopsy) by a single radiologist experienced in abdomen sonography. The radiologist was blinded to the final diagnosis and all other clinical and laboratory results. As shown in *Table 2*, left kidney length, width, and thickness, and cortical and medulla thickness were recorded using conventional US. Then, color Doppler imaging was applied to measure peak systolic velocity (PSV) and end-diastolic velocity (EDV) of the interlobar artery, with the sample volume located near the junction of renal cortex and medulla. After obtaining the measurements, the resistive index (RI) was calculated as an average of three to five waveforms.

MFI and imaging analysis

MFI was used to observe and record the vascular structures of renal cortical microcirculation. MFI parameters were

Table 1 Baseline characteristics of the study population (n=76)

Characteristic	Total	Healthy volunteers	MN patients	P value
Gender				0.35
Men	44	20 (45.5)	24 (54.5)	
Women	32	18 (56.3)	14 (43.8)	
Age (years)	51±13	48±12	54±13	0.05
BMI (kg/m²)	24.56±4.12	23.46±3.69	25.67±4.27	0.02
eGFR (mL/min)	102.20±28.83	118.53±23.17	85.87±26.82	<0.001
Scr (µmol/L)	78.74±68.93	59.53±6.11	97.95±93.99	<0.001
BUN (mmol/L)	5.69±2.44	4.69±0.84	6.70±3.05	<0.001

Data are presented as n, n (%), or mean ± standard deviation. MN, membranous nephropathy; BMI, body mass index; eGFR, estimated glomerular filtration rate; Scr, serum creatinine; BUN, blood urea nitrogen.

Table 2 Ultrasound characteristics of the study population

Variables	Heathy volunteers	MN patients	P value
Kidney length (mm)	100.71±6.71	106.08±8.33	0.004
Kidney width (mm)	44.32±5.08	49.63±4.68	<0.001
Kidney thickness (mm)	47.45±5.72	51.79±4.49	<0.001
Cortical thickness (mm)	5.28±1.12	5.36±1.08	0.76
Medulla thickness (mm)	10.41±1.86	10.35±2.20	0.77
PSV (cm/s)	31.5 [21–50]	30.5 [16–68]	0.41
EDV (cm/s)	14 [9–27]	13 [6–26]	0.031
RI	0.53±0.06	0.58±0.06	0.001
VI	0.65±0.09	0.35±0.18	<0.001
Vascular impression			<0.001
Good	33 (86.8)	5 (13.2)	
Intermediate	5 (20.8)	19 (79.2)	
Poor	0	14 (100.0)	
Vascular shape			<0.001
Normal	37 (68.5)	17 (31.5)	
Distorted	1 (6.3)	15 (93.8)	
Very distorted	0	6 (100.0)	

Data are presented as mean ± standard deviation, median [25–75%], or n (%). MN, membranous nephropathy; PSV, peak systolic velocity; EDV, end-diastolic velocity; RI, resistive index; VI, vascular index.

as follows: color velocity scale for color frequency was set at 2.5–3.0 MHz, and color gain was adjusted for optimal imaging. During examinations, the patients were requested to hold their breath at the end of inspiration to avoid motion artifacts caused by changes in breathing during MFI imaging. An MFI image of renal cortical microvasculature is shown in *Figure 2*. Then, features of the MFI image were assessed by the radiologist and another one who had not participated in performing the examination and was blinded to the results obtained by the former. The three indicators
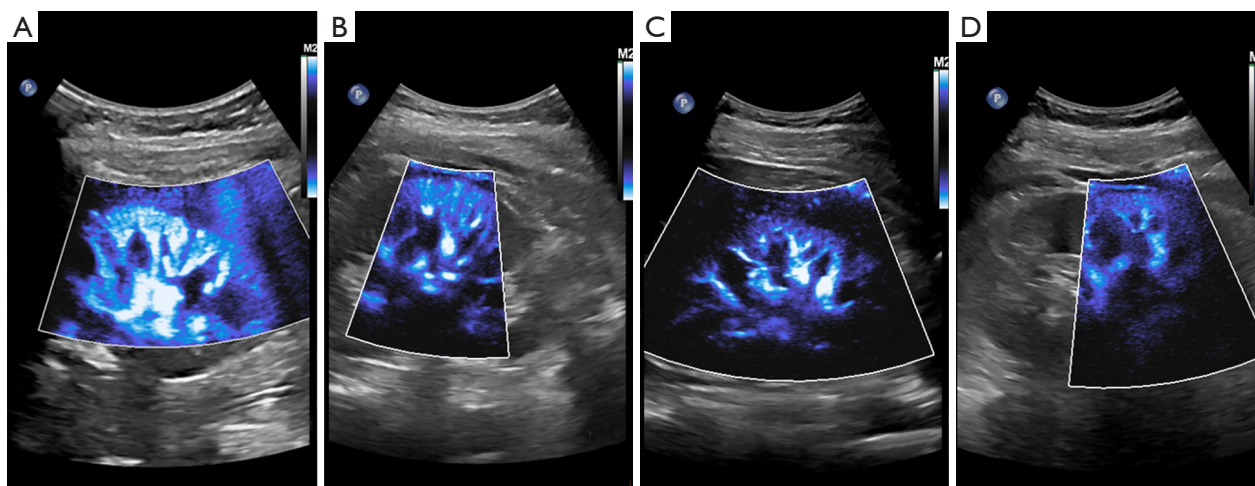
Figure 2 MFI ultrasound images of healthy controls and MN patients with varying degrees of vascular injury. (A) MFI image of a healthy volunteer; (B) MFI image of a patient with mild vascular damage; (C) MFI image of a patient with moderate vascular damage; (D) MFI image of a patient with severe vascular damage. MFI, MicroFlow imaging; MN, membranous nephropathy.

included impression, shape, and VI.

To standardize the interpretation, a 6-point semiquantitative analysis of each kidney was performed. The impression and shape of each patient's MFI image by radiologists have the rules of semi-quantitative scoring system, which was evaluated as follows: a kidney was considered good vascularity or a normal vessel when the final score was 5–6 on stage 1, stage 2 represented intermediate vascularity or a slightly distorted vessel when the final score was 3–4, and the kidney was poor vascularity or a considerably distorted vessel defined as a final score of 1–2 on stage 3 (23-25). Vascular filling was determined using the best image showing the quantity of vascular microcirculation. Then, we used an image-processing software Image Pro Plus to obtain the VI (*Figure 3*). The ROI we selected is located in the renal cortex of the middle part of the kidney, using the sector area of 1–3 interlobar artery branches. This measurement was done at least twice or the same patient. The ratio of this microcirculation value to the cross-sectional area of the renal cortex was measured as a percentage, and VI (Doppler signal pixels/pixels in the kidney) was calculated (*Table 2*) (15).

Two experienced observers analyzed separately. First, intra- and interobserver reproducibilities were evaluated. Second, discrepancies were resolved by consensus.

Evaluation of histopathology

After the kidney biopsy was performed, specimens obtained from the left kidney of each patient were immediately fixed in 4% paraformaldehyde, embedded in paraffin, serially sectioned, and stained with Periodic Acid-Schiff and Masson trichrome stains. All biopsies were evaluated using light microscopy by two renal pathologists. They assessed vascular damage based on glomerular lesions and arterioles, which were scored by the degree of glomerular sclerosis, vessel wall thickening and hyaloid degeneration of arterioles. Then, they assigned the semi-quantitative severity scores ranked into mild, moderate and severe group based on the degree of vascular sclerosis (26-28).

Statistical analysis

All statistical analyses were performed using SPSS 26 (IBM Corp., Armonk, New York, USA) and Python 3.9 (Python Software Foundation. Available on http://www.python.org). Student's *t*-test was used to compare differences between two parametric continuous variables. Analysis of variance (ANOVA) was used to compare differences among multiple groups. The Mann-Whitney *U* or Wilcoxon test was used to analyze non-parametric data, and the Chi-squared test was used to analyze categorical variables. Binary logistic regression (forward LR) and ordered logistic regression were used for multivariate analysis. Receiver operating characteristic (ROC) curve analysis was performed to assess diagnostic accuracy and was expressed as the area under the ROC curve (AUC). Comparisons between AUCs were made using the DeLong's test. The intra-class correlation
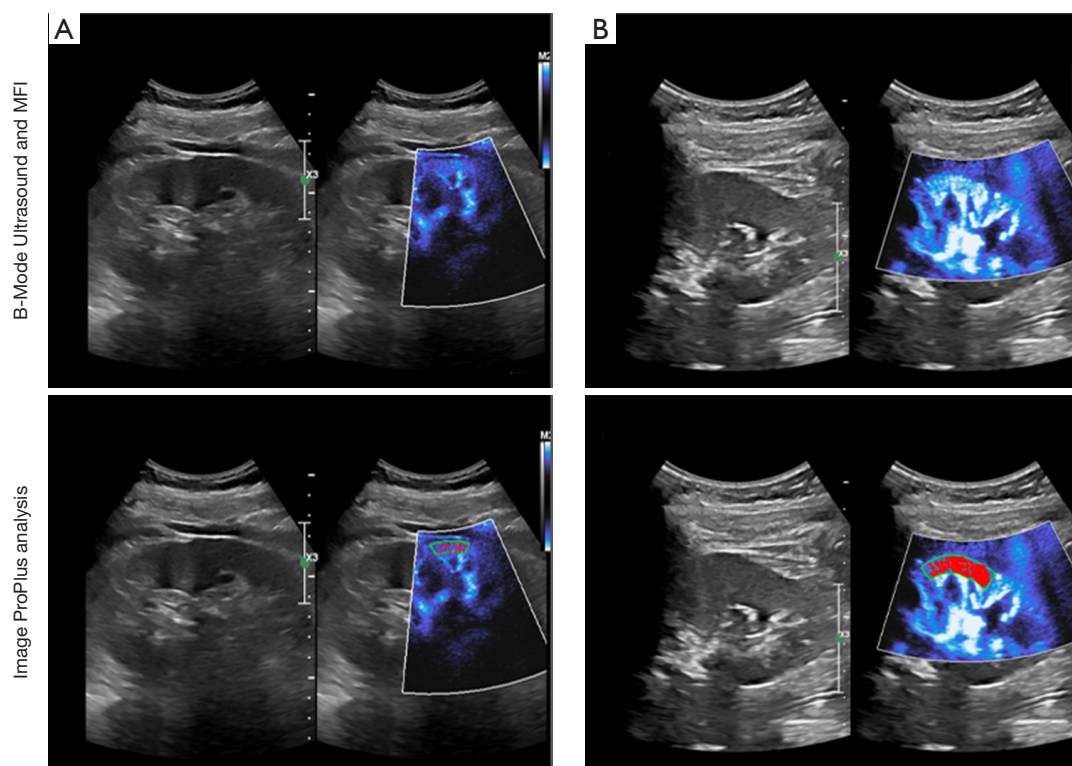
Figure 3 B-mode and MFI images of the left kidney in a MN patient and a healthy volunteer. The visualization and analysis of the ROIs in MFI mode were performed using Image Pro Plus. The VI is the ratio of Doppler signal pixels to total pixels in the ROI. (A) MN patient's left kidney analysis. (B) Healthy volunteer's left kidney analysis. Green area: ROI. Red area: cortical vascular area. MN, membranous nephropathy; MFI, MicroFlow imaging; VI vascular index; ROI, region of interest.

coefficients (ICCs) and Kappa coefficient were used to assess the reliability and consistency of the subjective evaluations of the VI, impression and shape of the MFI images. Chordal graphs and heat maps were used to visualize the relationship between all categorical and continuous variables and MN. Differences were considered statistically significant only when a two-sided P value was <0.05 in all tests.

Results

Characteristics of study participants

Thirty-eight patients with MN (54±13 years) and 38 healthy volunteers (48±12 years) were included in our present study. *Table 1* shows participant characteristics and the conducted laboratory tests. Our results show that there were scant statistical differences in age (P=0.05) and sex (P=0.35) between the patients and the controls. However, there was a slight difference in BMI between the two groups (P=0.02). Mean BMI of the patient group was 25.67±4.27 kg/m^2, which was

higher than that of the control group. The eGFR was lower in MN patients than in healthy controls (P<0.001). Conversely, the levels of serum creatinine (Scr) and blood urea nitrogen (BUN) were higher in MN patients than in healthy controls (all P<0.001). In addition, the MN group consisted of patients with diabetes (n=9) and hypertension (n=13).

US characteristics of participants

Renal parameters obtained using standard and MFI US are listed in *Table 2*. Compared with those of healthy volunteers, patients with MN in stage I–II tended to have larger kidneys including kidney length (P=0.004), width (P<0.001) and thickness (P<0.001); however, cortical thickness (P=0.76) and medulla thickness (P=0.77) did not show significant differences between the two groups of participants. Compared with those of healthy volunteers, all patients with MN showed a reduction in EDV (P=0.031) and an increase

in RI (P=0.001); however, PSV did not show significant differences between the two groups of participants (P=0.41). The intra- and inter-reader agreement was measured for the MFI images, regarding the intra-reader agreement and the ICCs ranged from 0.862 to 0.976; for the inter-reader agreement, the coefficient ranged from 0.756 to 0.870. The result of ICC can be found in the supplement (Table S1). Our results show that MFI could detect micro-vascularity within the renal cortex. VI was significantly lower in MN patients compared with that of healthy controls (0.65±0.09 *vs.* 0.35±0.18, P<0.001). Using MFI, we observed that the number of renal vascular impressions in MN patients with good, intermediate and poor impressions were 5 (13.2%), 19 (50.0%), and 14 (36.8%), respectively. In patients with MN, vascular shape was normal in 17 (44.7%), distorted in 15 (39.5%) and very distorted in 6 (15.8%) participants. Differences in VI, vascular impression levels, and vascular shape between healthy volunteers and MN patients were statistically significant (P<0.001).

All parameters with P<0.05 were analyzed using binary logistic regression (forward LR). It automatically selected the important independent variables among twelve parameters, only two were entered into the final model in the supplement (Figure S1). In the adjusted models, VI (P=0.001) was negatively and significantly associated with the presence of MN, while Scr levels (P=0.004) were positively and significantly indicative of MN (OR, 1.46E−11 [95% confidence interval (CI): 3.22E−18 to 6.60E−05]; OR, 1.176 (95% CI: 1.054–1.312, respectively).The exploratory diagnostic performance of VI (AUC: 0.94; 95% CI: 0.89–0.99) was superior to that of Scr (AUC: 0.87; 95% CI: 0.79–0.95). However, other parameters were not significantly associated with MN. In addition, Spearman correlation test was used to analyze the parameters for MN patients and healthy volunteers which can be found in the supplement (Table S2). A linear correlation was observed between the MN and the MFI parameters (VI, impression and shape), which means that MN correspond with abnormal ultrasonic parameters: VI (r=−0.76), impression (r=0.74) and shape (r=0.58). And this relationship was further visualized to show the connection between MFI parameters and MN (*Figure 4A,4B*).

Analysis of classification using pathologic vascular score

Based on the degree of renal vascular damage, we divided the 38 MN patients into mild (11 participants, 29%), moderate (15 participants, 40%) and severe (12 participants,

31%) groups.

Among the 38 participants with MN, differences in eGFR, VI, vascular impression levels and vascular shape were statistically significant (P<0.05); however, differences in other indicators were not statistically significant in these participants (P>0.05). Further details on participant characteristics are provided in *Table 3*. Because vascular impression levels and vascular shape were subjective parameters, we used the VI and eGFR for ordered logistic regression analysis. Finally, VI was identified as independent predictors of the degree of vascular changes in MN (P=0.012), whereas eGFR was not identified as such a predictor (P=0.105).

The diagnostic accuracy of predictor variables with P<0.05 in univariate logistic regression analysis is presented in the supplement (Table S3). The AUCs of the VI for different grades of vascular changes were 0.79 (mild, 95% CI: 0.64–0.94), 0.54 (moderate, 95% CI: 0.35–0.73) and 0.75 (severe, 95% CI: 0.59–0.90). Similarly, eGFR values were 0.63 (mild, 95% CI: 0.43–0.84), 0.60 (moderate, 95% CI: 0.41–0.78) and 0.75 (severe, 95% CI: 0.59–0.91). The vascular impression AUCs were 0.67 (mild, 95% CI: 0.47–0.87), 0.55 (moderate, 95% CI: 0.37–0.74) and 0.72 (severe, 95% CI: 0.55–0.90). In addition, AUCs for different grades of vascular changes in shape were 0.75 (mild 95% CI: 0.59–0.91), 0.51 (moderate, 95% CI: 0.32–0.70), and 0.74 (severe, 95% CI: 0.56–0.92). No statistical differences were observed among the different individual factors in the various groups (all P>0.05); however, in the mild vascular disease group, the AUCs of the VI were significantly higher than eGFR values. This may have been due to MFI having a high sensitivity for the vascular changes in MN patients in stages I–II, which facilitated the predictability of the VI. In addition, heat map and chordal graph (*Figure 4C,4D*) show correlation coefficients of the different parameters of vascular damage classifications in MN. Only the MFI-related parameters (VI r=−0.50, impression r=0.43, and shape r=0.52) and eGFR (r=−0.38) had a correlation with the degree of vascular damage (P<0.05) in the supplement (Table S4). Furthermore, the violin plot analysis shows the distribution of different US parameters and lab indexes in different groups (*Figure 5*).

Discussion

To the best of our knowledge, this is the first study to report on the predictive performance of a noninvasive examination using MFI in predicting the microvascular
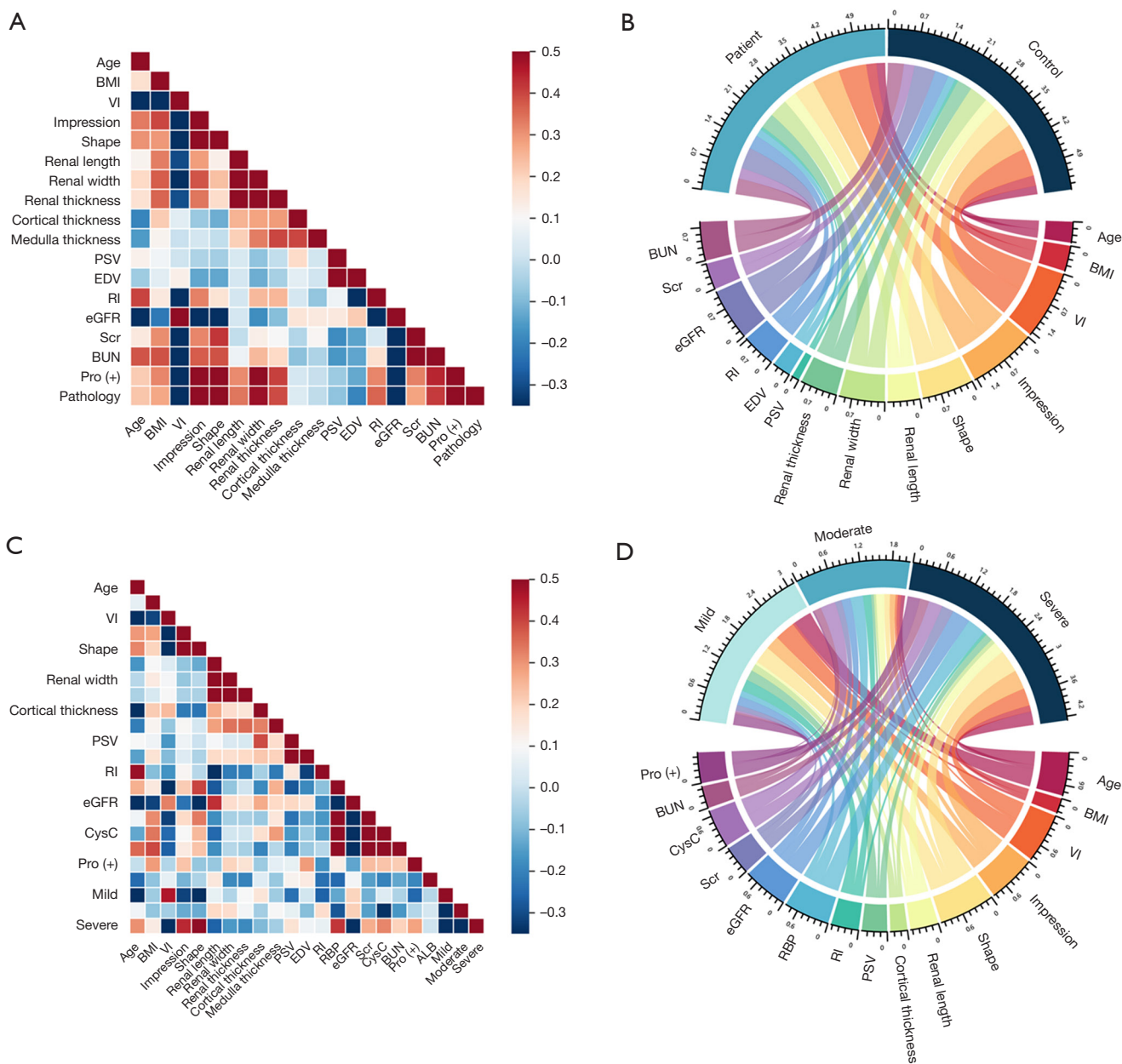
Figure 4 Heat map and chordal graphs were used to visualize the relationship between categorical parameters and MN. The abscissa and ordinate in (A) represent the 17 standardized features. (B) Relationship between all parameters and MN. The abscissa and ordinate in (C) represent the 20 feature signatures. (D) Relationship between all parameters and the pathology vascular score classification of MN. In the heat map, the darker the color, the closer the correlation coefficient value is to 1 or −1, and the more correlated the two features are. On the contrary, the lighter the color, the closer the correlation coefficient value is to 0, and the less correlated the two features are. The width of a link represents the strength of the correlation in the chordal graphs. BMI, body mass index; VI, vascular index; PSV, peak systolic velocity; EDV, end-diastolic velocity; RI, resistive index; eGFR, estimated glomerular filtration rate; Scr, serum creatinine; BUN, blood urea nitrogen; Pro (+), urine protein; CysC, cystatin C; ALB, albumin; RBP, retinol-binding protein.

Table 3 Pathology vascular score classification

Variables	Mild	Moderate	Severe	Univariate statistics, P value
N	11 (28.9)	15 (39.5)	12 (31.6)	
Gender				0.92
Men	7 (29.2)	10 (41.7)	7 (29.2)	
Women	4 (28.6)	5 (35.7)	5 (35.7)	
Age (years)	52 [32–65]	56 [39–70]	55 [52–74]	0.06
BMI (kg/m^2)	25.29±3.90	25.27±3.69	26.53±5.39	0.72
Hypertension	4 (30.8)	5 (38.5)	4 (30.8)	0.98
Diabetes	1 (11.1)	4 (44.4)	4 (44.4)	0.37
RI	0.55±0.04	0.59±0.07	0.58±0.07	0.27
Kidney length (mm)	106.91±7.29	108±9.34	102.92±7.60	0.27
Kidney width (mm)	49.36±4.65	50.67±4.53	48.58±5.02	0.52
Kidney thickness (mm)	52.45±3.80	52.27±4.54	50.58±5.11	0.54
Cortical thickness (mm)	5.62±1.19	5.29±1.15	5.20±0.92	0.63
Medulla thickness (mm)	10.15±2.08	10.63±2.59	10.18±1.90	0.83
PSV (cm/s)	27 [22–37]	31 [16–47]	27.5 [20–68]	0.35
EDV (cm/s)	12 [9.5–26]	13 [6–26]	11.5 [9–25]	0.85
eGFR (mL/min)	94.19±28.09	92.64±22.74	69.78±25.09	0.037
Scr (μmol/L)	88 [49–118]	75.5 [54–95]	105 [66–643]	0.21
BUN (mmol/L)	7.2 [4–12.2]	5.8 [2.2–7.8]	6.25 [4.6–18.7]	0.66
CysC (mg/L)	1.38 [0.61–3.3]	1.06 [0.61–1.38]	1.53 [0.89–4.9]	0.12
RBP (mg/L)	37 [31–55]	43 [31–58]	46.5 [38–129]	0.20
ALB (g/L)	28.56±11.65	29.30±11.59	29.13±12.22	0.99
Pro (+)				0.40
(++)	3 (60.0)	2 (40.0)	0	
(+++)	6 (27.3)	9 (40.9)	7 (31.8)	
(++++)	2 (18.2)	4 (36.4)	5 (45.5)	
VI	0.48±0.13	0.34±0.18	0.25±0.15	0.006
Vascular impression				0.007
Good	4 (80.0)	1 (20.0)	0	
Intermediate	4 (21.1)	11 (57.9)	4 (21.1)	
Poor	3 (21.4)	3 (21.4)	8 (57.1)	
Vascular shape				0.013
Normal	8 (47.1)	7 (41.2)	2 (11.8)	
Distorted	3 (20.0)	7 (46.7)	5 (33.3)	
Very distorted	0	1 (16.7)	5 (83.3)	

Data are presented as n (%), mean ± standard deviation, or median [25–75%]. BMI, body mass index; RI, resistive index; PSV, peak systolic velocity; EDV, end-diastolic velocity; eGFR, estimated glomerular filtration rate; Scr, serum creatinine; BUN, urea nitrogen; CysC, cystatin C; RBP, retinol-binding protein; ALB, albumin; Pro (+), urine protein; VI, vascular index.
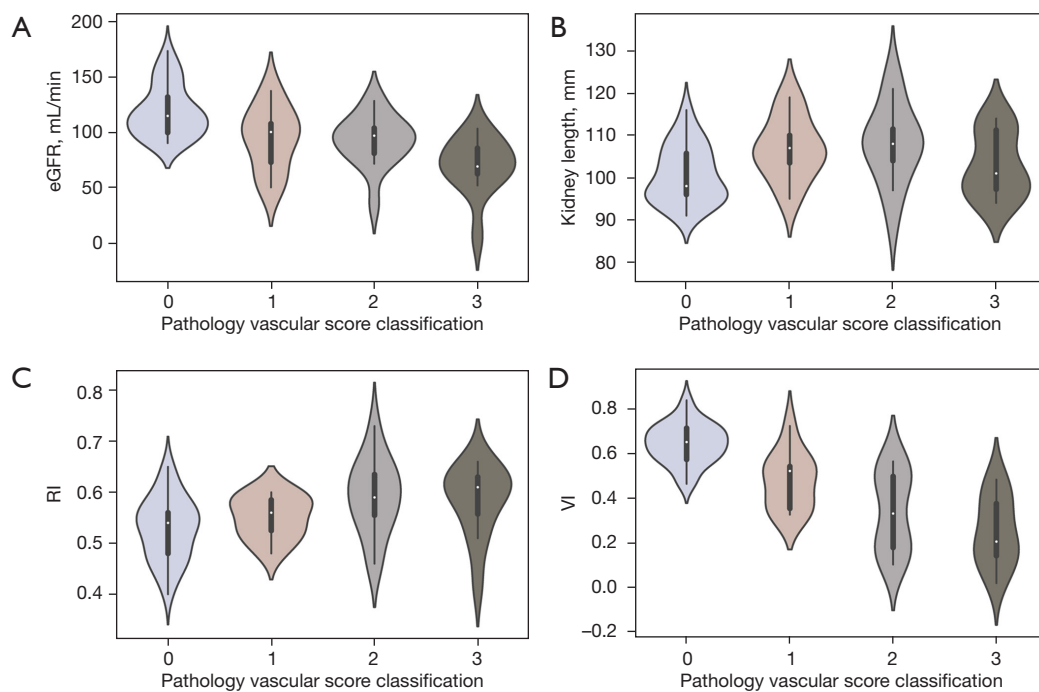
Figure 5 Violin graphs visualize the relationship between continuous parameters and MN pathology vascular score; 0= none (n=38); 1= mild (n=11); 2= moderate (n =15); and 3= severe (n=12). (A) Relationship between eGFR and MN pathology vascular score. (B) Relationship between kidney length and MN pathology vascular score. (C) Relationship between RI and MN pathology vascular score. (D) Relationship between VI and MN pathology vascular score. eGFR, estimated glomerular filtration rate; RI, resistive index; VI, vascular index; MN, membranous nephropathy.

damage of the chronic kidney disease MN. In this study, we demonstrated the feasibility of MFI for the detection of early-stage vascular changes in MN among MN patients in stages I–II (and particularly in early-stage patients), who have not yet shown changes in eGFR or Scr levels. Specifically, we have shown that the VI detected using MFI was significantly lower in MN patients compared with that in healthy controls. In binary logistic regression analysis, VI and Scr levels were identified as independent predictors of MN. MFI showed good diagnostic performance (AUC: 0.94, 95% CI: 0.89–0.99) in identifying participants with stages I–II MN. A previous study has indicated that kidney length is commonly used for clinical monitoring of kidney damage (29). Yaprak *et al.* measured the renal cortical thickness of 120 patients with CKD stages 1–5, and the results showed that the thickness of the renal cortex was positively correlated with eGFR (30). Petrucci *et al.* hold that RI is an indirect measure of microcirculation impedance, which increases when arteriolosclerosis and microcirculation rarefaction occur (31). We also reached the same conclusion. Surprisingly, MFI outperformed other US

imaging markers including kidney length (AUC: 0.69; 95% CI: 0.57–0.81) and RI (AUC: 0.71; 95% CI: 0.59–0.83), and biochemical criterions such as Scr levels (AUC: 0.87; 95% CI: 0.79–0.95). Similarly, MFI also detected the stages of microvascular damage among patients who had undergone a kidney biopsy. All the radiological parameters of MFI (index, impression, and shape) were dramatically different among the three grades (P<0.05). We found that all predictors had lower AUCs in the moderate group than the other groups. This could be due to two reasons: our small sample size, which could cause bias; and our selection of some moderate patients who were close to the threshold of adjacent groups, which could affect the evaluation of the moderate group. In the group with mild vascular damage, however, VI showed better predictive performance than those of other parameters in the preliminary detection of microcirculatory damage.

MN is a common cause of pathologic nephrotic syndrome and kidney failure. The frequency of MN remains steady in China. Current guidelines recommend screening all patients with nephrotic syndrome using renal biopsy.

However, this approach is hampered by lack of compliance stemming from the invasiveness of this examination (32,33). Currently, MFI is used as an innovative US-based additional tool for grayscale, color, and spectral Doppler evaluation of incidentally detected kidney injury. MFI offers an increased level of detail and improved visualization of small branching vessels by combining approaches such as flash, motion suppression and other artifact-reducing techniques with adaptive filtering to remove clutter; this technique improves sensitivity to slow-flow Doppler signals (19,22,34). Using MFI, we have found that the cortical VI of MN patients was significantly lower than that of healthy controls (0.65±0.09 vs. 0.35±0.18, P<0.01) in our present study, which is consistent with the findings of Armaly et al. (23). Using CEUS, Garessus et al. obtained similar results in patients with chronic kidney disease (35). The kidney contains a complex network of blood vessels, consisting of glomerular and peritubular capillaries. Entering the kidney at the hilum and branching into smaller arteries, the renal artery repeatedly divides into interlobar, arcuate and interlobular arteries. Blood is supplied to the glomerular capillaries, which make up the kidney's capillary network, by afferent arterioles that mostly originate from interlobular arteries (36,37). The pathologic changes in MN include thickened capillary walls, arteriolosclerosis and characteristic immune-complex deposits along the glomerular basement membranes (1,3,38). Damage to glomerular capillary walls and arteriole can alter renal blood flow and lead to a progressive decrease in peritubular capillary flow, resulting in mild tubulointerstitial ischemia. This cascade of events may be both a cause and/or consequence of renal fibrosis and kidney insufficiency (37,39). Furthermore, we observed obvious differences in VI among the three groups of MN patients with mild changes compared with the reference standard renal biopsy. This finding indicates a strong correlation between the result of the biopsy and VI in diseased patients. This finding also supports the reliability of MFI and demonstrates its ability to show a decrease in kidney vascular damage, especially in the mild stages. In addition, we found that the VI declined among some early MN patients even though there were no major changes in Scr, which may have been attributed to remaining healthy nephrons underwent functional changes to compensate for the loss of diseased nephrons and maintain homeostasis of kidney until approximately 75% of nephrons are lost (40). The eGFR in daily clinical practice is not always consistent with the histopathologic changes and insensitive to subclinical injury (41-43). Armaly and his team also found the decline of VI in the early diagnosis even without major changes in

Scr (23). Moreover, using multiple quantitative measures, we have demonstrated that MFI showed a higher sensitivity than those of other US technologies, such as kidney length and RI in visualizing the kidney cortical microvasculature to predict MN. These results show that MFI is a convenient, noninvasive and accurate approach that can be used to predict MN without the use of a contrast agent and can be helpful in patient follow-up and clinical decision-making.

Despite these encouraging results, our current study had several limitations. First, the number of patients and controls was small. Hence, a larger follow-up study is needed to confirm our findings. Second, the reliability of MFI may have been influenced by different operators. Therefore, a standardized MFI measurement was used in this study, and ultrasonic examination was performed by experienced US doctors to minimize the potential subjective interference. Third, even though MFI has multiple uses, its diagnostic utility is rather limited, as it cannot tell apart different forms of vascular damage. In addition, our sample size was small. Therefore, we did not perform subgroup analysis on patients with other diseases (such as diabetes, hypertension, renal artery stenosis, etc.). In the future, we will continue to collect patients for further exploration.

Conclusions

In conclusion, our results showed that MFI, which is a microvascular full-field-of-view imaging method, showed promise in the noninvasive prediction of MN, especially in early disease with preserved renal function. Combining the VI of MFI with conventional B-mode US improved the differentiation of healthy kidneys from those affected by MN. VI, which is a highly reproducible quantitative parameter of MFI, may provide additional objective information, which would be useful for detecting renal changes in MN during early detection and assessing the severity of MN and treatment options during follow-up.

Acknowledgments

Footnote

Reporting Checklist: The authors have completed the STARD reporting checklist. Available at https://qims.amegroups.

com/article/view/10.21037/qims-23-1010/rc

Conflicts of Interest: All authors have completed the ICMJE uniform disclosure form (available at https://qims. amegroups.com/article/view/10.21037/qims-23-1010/coif). The authors have no conflicts of interest to declare.

Ethical Statement: The authors are accountable for all aspects of the work in ensuring that questions related to the accuracy or integrity of any part of the work are appropriately investigated and resolved. The study was conducted in accordance with the Declaration of Helsinki (as revised in 2013). The study was approved by the Ethical Committee of the First Hospital of Jilin University. Written informed consent for a native kidney biopsy and participation in the study in its entirety was obtained from all the study participants.

Open Access Statement: This is an Open Access article distributed in accordance with the Creative Commons Attribution-NonCommercial-NoDerivs 4.0 International License (CC BY-NC-ND 4.0), which permits the non-commercial replication and distribution of the article with the strict proviso that no changes or edits are made and the original work is properly cited (including links to both the formal publication through the relevant DOI and the license). See: https://creativecommons.org/licenses/by-nc-nd/4.0/.

References

1. Ronco P, Beck L, Debiec H, Fervenza FC, Hou FF, Jha V, Sethi S, Tong A, Vivarelli M, Wetzels J. Membranous nephropathy. Nat Rev Dis Primers 2021;7:69.
2. Ronco P, Debiec H. Molecular Pathogenesis of Membranous Nephropathy. Annu Rev Pathol 2020;15:287-313.
3. Gu Y, Xu H, Tang D. Mechanisms of Primary Membranous Nephropathy. Biomolecules 2021;11:513.
4. Couser WG. Primary Membranous Nephropathy. Clin J Am Soc Nephrol 2017;12:983-97.
5. Hou JH, Zhu HX, Zhou ML, Le WB, Zeng CH, Liang SS, Xu F, Liang DD, Shao SJ, Liu Y, Liu ZH. Changes in the Spectrum of Kidney Diseases: An Analysis of 40,759 Biopsy-Proven Cases from 2003 to 2014 in China. Kidney Dis (Basel) 2018;4:10-9.
6. Beck LH Jr, Bonegio RG, Lambeau G, Beck DM, Powell DW, Cummins TD, Klein JB, Salant DJ. M-type phospholipase A2 receptor as target antigen in idiopathic membranous nephropathy. N Engl J Med 2009;361:11-21.
7. Radice A, Pieruzzi F, Trezzi B, Ghiggeri G, Napodano P, D'Amico M, Stellato T, Brugnano R, Ravera F, Rolla D, Pesce G, Giovenzana ME, Londrino F, Cantaluppi V, Pregnolato F, Volpi A, Rombolà G, Moroni G, Ortisi G, Sinico RA. Diagnostic specificity of autoantibodies to M-type phospholipase A2 receptor (PLA2R) in differentiating idiopathic membranous nephropathy (IMN) from secondary forms and other glomerular diseases. J Nephrol 2018;31:271-8.
8. Luo J, Zhang W, Su C, Zhou Z, Wang G. Seropositive PLA2R-associated membranous nephropathy but biopsy-negative PLA2R staining. Nephrol Dial Transplant 2021;36:2216-23.
9. Svobodova B, Honsova E, Ronco P, Tesar V, Debiec H. Kidney biopsy is a sensitive tool for retrospective diagnosis of PLA2R-related membranous nephropathy. Nephrol Dial Transplant 2013;28:1839-44.
10. Fogo AB, Lusco MA, Najafian B, Alpers CE. AJKD Atlas of Renal Pathology: Immunotactoid Glomerulopathy. Am J Kidney Dis 2015;66:e29-30.
11. Grossmann M, Tzschätzsch H, Lang ST, Guo J, Bruns A, Dürr M, Hoyer BF, Grittner U, Lerchbaumer M, Nguyen Trong M, Schultz M, Hamm B, Braun J, Sack I, Marticorena Garcia SR. US Time-Harmonic Elastography for the Early Detection of Glomerulonephritis. Radiology 2019;292:676-84.
12. Çildağ MB, Gök M, Abdullayev O. Pre-procedural shear wave elastography on prediction of hemorrhage after percutaneous real-time ultrasound-guided renal biopsy. Radiol Med 2020;125:784-9.
13. Kajawo S, Ekrikpo U, Moloi MW, Noubiap JJ, Osman MA, Okpechi-Samuel US, Kengne AP, Bello AK, Okpechi IG. A Systematic Review of Complications Associated With Percutaneous Native Kidney Biopsies in Adults in Low- and Middle-Income Countries. Kidney Int Rep 2021;6:78-90.
14. Lee EJ, Chang YW, Oh E, Hwang J, Kim HJ, Hong SS. Reproducibility and diagnostic performance of the vascular index of superb microvascular imaging in real-time breast ultrasonography for evaluating breast masses. Ultrasonography 2021;40:398-406.
15. Yildiran G, Seher N, Sutcu M, Nayman A, Akdag O, Tosun Z. Median Nerve's Microcirculation in Carpal Tunnel Syndrome: Superb Microvascular Imaging. Plast Reconstr Surg 2021;147:1355-60.
16. Goudot G, Berkane Y, de Clermont-Tonnerre E, Guinier C, Filz von Reiterdank I, van Kampen A,

Uygun K, Cetrulo CL Jr, Uygun BE, Dua A, Lellouch AG. Microvascular assessment of fascio-cutaneous flaps by ultrasound: A large animal study. Front Physiol 2022;13:1063240.

17. Yang F, Zhao J, Liu C, Mao Y, Mu J, Wei X, Jia J, Zhang S, Xin X, Tan J. Superb microvascular imaging technique in depicting vascularity in focal liver lesions: more hypervascular supply patterns were depicted in hepatocellular carcinoma. Cancer Imaging 2019;19:92.

18. Gürbüz AF, Keven A, Elmalı A, Toru S, Apaydın A, Çeken K. A comparison between the superb microvascular imaging technique and conventional Doppler ultrasound in evaluating chronic allograft damage in renal transplant recipients. Diagn Interv Radiol 2023;29:212-8.

19. Zamani M, Skagen K, Scott H, Lindberg B, Russell D, Skjelland M. Carotid Plaque Neovascularization Detected With Superb Microvascular Imaging Ultrasound Without Using Contrast Media. Stroke 2019;50:3121-7.

20. Hernández-Socorro CR, Saavedra P, López-Fernández JC, Lübbe-Vazquez F, Ruiz-Santana S. Novel High-Quality Sonographic Methods to Diagnose Muscle Wasting in Long-Stay Critically Ill Patients: Shear Wave Elastography, Superb Microvascular Imaging and Contrast-Enhanced Ultrasound. Nutrients 2021;13:2224.

21. Wang Y, Yao M, Zou M, Ge Z, Cai S, Hong Y, Gao L, Zhang L, Dong Y, Peng B, Wang H, Li J. Relationship Between Serum Lipid Profiles and Carotid Intraplaque Neovascularization in a High-Stroke-Risk Population: A Cross-Sectional Study in China. J Am Heart Assoc 2021;10:e021545.

22. Aziz MU, Eisenbrey JR, Deganello A, Zahid M, Sharbidre K, Sidhu P, Robbin ML. Microvascular Flow Imaging: A State-of-the-Art Review of Clinical Use and Promise. Radiology 2022;305:250-64.

23. Armaly Z, Abu-Rahme M, Kinaneh S, Hijazi B, Habbasshi N, Artul S. An Innovative Ultrasound Technique for Early Detection of Kidney Dysfunction: Superb Microvascular Imaging as a Reference Standard. J Clin Med 2022;11:925.

24. Hitzel A, Liard A, Dacher JN, Gardin I, Ménard JF, Manrique A, Véra P. Quantitative analysis of 99mTc-DMSA during acute pyelonephritis for prediction of long-term renal scarring. J Nucl Med 2004;45:285-9.

25. Chen Q, Yu J, Rush BM, Stocker SD, Tan RJ, Kim K. Ultrasound super-resolution imaging provides a noninvasive assessment of renal microvasculature changes during mouse acute kidney injury. Kidney Int 2020;98:355-65.

26. Srivastava A, Palsson R, Kaze AD, Chen ME, Palacios P,

Sabbisetti V, Betensky RA, Steinman TI, Thadhani RI, McMahon GM, Stillman IE, Rennke HG, Waikar SS. The Prognostic Value of Histopathologic Lesions in Native Kidney Biopsy Specimens: Results from the Boston Kidney Biopsy Cohort Study. J Am Soc Nephrol 2018;29:2213-24.

27. Yang WQ, Mou S, Xu Y, Xu L, Li FH, Li HL. Quantitative parameters of contrast-enhanced ultrasonography for assessment of renal pathology: A preliminary study in chronic kidney disease. Clin Hemorheol Microcirc 2018;68:71-82.

28. Katafuchi R, Kiyoshi Y, Oh Y, Uesugi N, Ikeda K, Yanase T, Fujimi S. Glomerular score as a prognosticator in IgA nephropathy: its usefulness and limitation. Clin Nephrol 1998;49:1-8.

29. The AIUM Practice Parameter for the Performance of an Ultrasound Examination of the Abdomen and/or Retroperitoneum. J Ultrasound Med 2022;41:E1-8.

30. Yaprak M, Çakır Ö, Turan MN, Dayanan R, Akın S, Değirmen E, Yıldırım M, Turgut F. Role of ultrasonographic chronic kidney disease score in the assessment of chronic kidney disease. Int Urol Nephrol 2017;49:123-31.

31. Petrucci I, Clementi A, Sessa C, Torrisi I, Meola M. Ultrasound and color Doppler applications in chronic kidney disease. J Nephrol 2018;31:863-79.

32. Floege J, Barbour SJ, Cattran DC, Hogan JJ, Nachman PH, Tang SCW, Wetzels JFM, Cheung M, Wheeler DC, Winkelmayer WC, Rovin BH; . Management and treatment of glomerular diseases (part 1): conclusions from a Kidney Disease: Improving Global Outcomes (KDIGO) Controversies Conference. Kidney Int 2019;95:268-80.

33. Hofstra JM, Fervenza FC, Wetzels JF. Treatment of idiopathic membranous nephropathy. Nat Rev Nephrol 2013;9:443-58.

34. Lee S, Lee JY, Yoon RG, Kim JH, Hong HS. The Value of Microvascular Imaging for Triaging Indeterminate Cervical Lymph Nodes in Patients with Papillary Thyroid Carcinoma. Cancers (Basel) 2020;12:2839.

35. Garessus J, Brito W, Loncle N, Vanelli A, Hendriks-Balk M, Wuerzner G, Schneider A, Burnier M, Pruijm M. Cortical perfusion as assessed with contrast-enhanced ultrasound is lower in patients with chronic kidney disease than in healthy subjects but increases under low salt conditions. Nephrol Dial Transplant 2022;37:705-12.

36. Tanabe K, Wada J, Sato Y. Targeting angiogenesis and lymphangiogenesis in kidney disease. Nat Rev Nephrol 2020;16:289-303.

37. Chade AR. Renal vascular structure and rarefaction.

Compr Physiol 2013;3:817-31.

38. Fogo AB. Milk and membranous nephropathy. N Engl J Med 2011;364:2158-9.

39. Sun D, Eirin A, Ebrahimi B, Textor SC, Lerman A, Lerman LO. Early atherosclerosis aggravates renal microvascular loss and fibrosis in swine renal artery stenosis. J Am Soc Hypertens 2016;10:325-35.

40. Orr SE, Bridges CC. Chronic Kidney Disease and Exposure to Nephrotoxic Metals. Int J Mol Sci 2017;18:1039.

41. Zhang WR, Parikh CR. Biomarkers of Acute and Chronic

Kidney Disease. Annu Rev Physiol 2019;81:309-33.

42. Zhu M, Ma L, Yang W, Tang L, Li H, Zheng M, Mou S. Elastography ultrasound with machine learning improves the diagnostic performance of traditional ultrasound in predicting kidney fibrosis. J Formos Med Assoc 2022;121:1062-72.

43. Rysz J, Gluba-Brzózka A, Franczyk B, Jabłonowski Z, Ciałkowska-Rysz A. Novel Biomarkers in the Diagnosis of Chronic Kidney Disease and the Prediction of Its Outcome. Int J Mol Sci 2017;18:1702.